Environ. Sci. Technol. **1999**, *33,* 2247−2251

Collision Frequencies of Fractal Bacterial Aggregates with Small Particles in a Sheared Fluid

TERESA SERRA† AND BRUCE E. LOGAN*,‡

Department of Physics, University of Girona, Girona, Spain, and Department of Civil and Environmental Engineering, The Pennsylvania State University, University Park, Pennsylvania 16802

Bacteria were aggregated in a paddle mixer, producing highly amorphous aggregates of 3−300 μm diameter with an average fractal dimension of $D = 2.52$. To determine the rate that these types of biological flocs could coagulate with other particles, collision frequencies of these aggregates with small (0.49 μm diameter) fluorescent yellow green (YG) latex microspheres were measured in a paddle mixer at a mean shear rate of 17 s^{-1}. As the aggregate sizes (<5 μm) approached that of the small YG microspheres, measured collision rates converged to values similar to those predicted by two conventional coagulation models (rectilinear and curvilinear) developed for collisions between spherical particles. Collision frequencies between larger bacterial aggregates (L_a ~100 μm) and YG microspheres were found to be as much as 2 orders of magnitude smaller than values predicted using a rectilinear coagulation model but 5 orders of magnitude higher than predicted using the curvilinear model. Similar but slightly larger collision frequencies were obtained for aggregates ($D = 2.31$) made from red-stained microspheres (2.93 μm diameter). These data when combined with other data for larger inorganic aggregates indicate that the collision function increases from 10^{-10} to 10^{-6} cm^3 s^{-1} for fractal aggregates 3−1000 μm in size with small particles. These results demonstrate that fractal aggregates of particles collide much more frequently than expected based on spherical-particle coagulation models and suggest that coagulation rates in natural systems are much more rapid than predicted by coagulation models based on impermeable spheres.

Introduction

Particle coagulation is a critical factor in the transport of dissolved and particulate matter in natural and engineered systems. In the ocean, for example, individual bacteria and phytoplankton settle too slowly to reach deep sediments. The downward flux of organic carbon in the ocean is therefore dominated by large aggregate sedimentation (*1, 2*). This loss of organic carbon, which is made possible by coagulation, is an important component of global atmospheric carbon dioxide. During settling, marine aggregates continue to scavenge other particles and increase the overall loss of carbon from the system. Settling and sheared aggregates of particles can also scavenge dissolved and colloidal material (*3, 4*) and have been shown to control the sorption of metals by suspended particles and therefore their transport throughout the water column (*5*).

Despite the importance of coagulation processes, the rate at which particles collide in aqueous systems is not well-known. Early (*6*) and later (*7*) models predicted collision rates in proportion to the maximum possible overlap between approaching particles due to Brownian motion, fluid shear, and differential sedimentation (rectilinear coagulation model). Subsequent mathematical formulations, referred to as curvilinear models, have been developed to account for various hydrodynamic and electrostatic effects to more accurately describe the actual frequency of collisions of spherical particles (*8, 9*). As the particle sizes become increasingly dissimilar, curvilinear models predict rapidly decreasing collision frequencies while the rectilinear models predict increasing collision frequencies.

Particles produced by aggregation are not usually spheres but highly amorphous, nonspherical, and fractal with three-dimensional fractal dimensions spanning a range from ~1.5 to the maximum of 3 (*10*−*13*). The open structure of fractal aggregates permits fluid flow through the aggregate, allowing greater collision frequencies between dissimilar sized particles than predicted by curvilinear models based on impermeable spheres.

The capture of small particles by individual fractal aggregates ranging in size from 200 to 1000 μm and composed of latex microspheres was recently examined for settling aggregates and for aggregates in a sheared fluid (*4, 14*). Collision frequencies were found to be 5 orders of magnitude higher than predicted using the curvilinear model of Han and Lawler (*8*). The generality of these findings needs to be established for other types of fractal aggregates and for particles spanning a larger size range. Many aggregates in natural and engineered systems, for example, are composed of organic matter such as bacteria and phytoplankton. Exopolymeric material produced by these microorganisms can occupy spaces between the cells (*15, 16*), altering the porosity and permeability of these biological flocs relative to those composed of latex microspheres.

To examine the collision frequencies between microbiological aggregates and other particles in the water column, we measured the collision rate of bacterial aggregates (flocs) with fluorescent microspheres. Collision frequencies calculated for these flocs were compared with those obtained for inorganic aggregates (latex microspheres) ranging in size from 3 to 300 μm and with those of Li and Logan (*14*) for larger (200−1000 μm) microsphere aggregates.

Methods

Bacterial Aggregates. A bacterial suspension was developed using activated sludge supernatant from The Pennsylvania State University wastewater treatment plant. The supernatant (5 vol %) was incubated for 24 h at room temperature (20−23 °C) using a medium consisting of BOD dilution water (BOD nutrient pillows, Hach Co.) and a mixture of glucose, glutamic acid, and dextran (250 mg/L each). The suspension was aerated by rapid stirring using a stir bar.

To form bacterial aggregates, a portion of this suspension (80 mL) was added to a 1-L beaker filled to 520 mL with deionized water (Milli-Q water, Millipore Corp.) containing a polymer coagulant (7 mg/L; Praestol 2520, Stockhausen Inc.). This solution was coagulated at 30 rpm using a standard jar-test apparatus (model 7790-400, Phipps and Bird) equipped with flat paddles (7.6 × 2.5 cm^2).

* Corresponding author phone: (814)863-7908; fax: (814)863-7304; e-mail: blogan@psu.edu.
† University of Girona.
‡ The Pennsylvania State University.

10.1021/es981125v CCC: $18.00
Published on Web 05/20/1999

Microsphere Aggregates. Inorganic aggregates were formed using red-dyed latex beads (RB) having a mean diameter of 2.93 μm and a density of 1.05 mg/L (Polysciences) as previously described (*4*). Briefly, RB ($\sim 10^7$ mL^{-1}) were added to 200 mL of deionized water containing NaCl (2%) at a pH ~8.5 and coagulated for 24 h using the jar-test device set at a mixing speed of 10 rpm.

Coagulation Experiments with Aggregates. Coagulation experiments were performed by combining suspensions of aggregates with suspensions ($\sim 10^7$ mL^{-1}) of fluorescent yellow-green (YG) beads (0.49 μm diameter, density of 1.05 g/mL; Polysciences). The suspension of beads and aggregates (0.6 L) was stirred using the paddle mixer at 30 rpm, equal to a mean shear rate of 17 s^{-1} based on a correlation in Li and Logan (*4*). Samples (0.1 mL of bacterial or 0.6 mL of microsphere aggregate suspensions) were taken over time (0−40 min) using a 1-mL pipet tip cut midway between its ends to provide a larger opening to avoid disruption of the aggregates. For experiments with bacteria, samples were transferred into a filtration funnel containing 10 mL of MilliQ water and a black filter (0.2 μm pore diameter; Poretics Corp.) and stained with a fluorescent dye (acridine orange, 0.1% final concentration containing 2% of formaldehyde) for 5 min. For experiments with microsphere RB aggregates, samples were transferred directly to the funnel for filtration without staining. Samples were analyzed under blue light using a microscope (Olympus BH2) and image analysis system (Galai) (*18*). Aggregate sizes (L_a) were based on projected area (A) measured using the image analysis system, where $L_a = (4A/\pi)^{1/2}$.

The coagulation rate was calculated by directly counting the number of YG beads attached to aggregates as a function of time (see below). YG beads did not significantly coagulate during experiments at the polymer concentration and ionic strength concentrations used in experiments. This technique is the same one used by Li and Logan (*14*), except that in their study individual macroscopic aggregates were added into a beaker containing YG beads and the same aggregates were removed at different times. Here, suspensions of aggregates and beads were combined, and samples containing a large distribution of aggregate sizes were recovered.

Fractal Dimensions. Average fractal dimensions of aggregates were calculated using the particle concentration technique (PCT) (*18*−*20*). In this method, the fractal dimension can be calculated by measuring cumulative size distributions (N) in terms of both actual length (L_a) and solid volume (v_s) for the same population of particles. The volume can be converted to a length scale using $v_s = \pi d_s^3$, where d_s is the solid equivalent diameter, defined as the size that the aggregate would have if it was spherical and had no porosity. As a result, d_s is always less than L_a. The cumulative length size distribution, $N(L_a)$, was obtained using the image analysis system by scanning ~100 microscope fields of a slide at 100× and 40×. A Coulter-Counter (Coulter Multisizer II, Coulter Corp.) with an aperture of 100 μm was used to measure the solid volume distribution of the particles, resulting in a measurable size range from $2 \le d_s \le 60$ μm.

The fractal dimension is related to the solid and actual lengths of aggregates (*19*) by

$$d_s = C L_a^{D/3} \tag{1}$$

The aggregate size (L_a) that corresponds to the solid equivalent diameter (d_s) can be identified using the two cumulative size distributions. Particle sizes can be matched when the number of particles in the one of the cumulative distributions is the same as in the other distribution or when $N(L_a) = N(d_s)$. A series of points are therefore matched for several different values of the characteristic length and solid diameter. Using eq 1, the slope of a log−log plot of the paired values of d_s and L_a can be used to calculate the value of the fractal dimension D.

Calculation of the Collision Frequency Function. The rate at which a particle, p, collides with an individual aggregate, a, can be calculated (*14*) as

$$R_c = \alpha(a,p)\beta(a,p)N_p \tag{2}$$

where N_p is the concentration of small particles, $\beta(a,p)$ is the collision frequency function, and $\alpha(a,p)$ is the collision efficiency for the coagulation between a particle and an aggregate defined as the ratio of the particles that stick to each other to the rate at which they collide. This rate is assumed to be constant during a short exposure time of the coagulation experiment with aggregates and particles. For a constant collision rate, the number of particles captured by the aggregate, P_c, can be calculated as $P_c = R_c t$. Therefore β can be calculated from

$$\beta = \frac{P_c}{\alpha t N_p} \tag{3}$$

The collision efficiency was measured between individual YG and red beads as described in Li and Logan (*4*). Briefly, monodisperse suspensions of YG ($N_{YG} = 6.4 \times 10^5$ mL^{-1}) and red beads ($N_r = 1.0 \times 10^5$ mL^{-1}) were prepared and coagulated at a mean shear rate of 20 s^{-1} using the same NaCl concentration as in the aggregate coagulation experiments. Under these conditions, the YG beads were relatively stable, and the number of collisions between RB and YG beads was higher than the number of collisions between RB. The rectilinear collision efficiency was calculated as $\alpha_{rec} = 0.769$ using the rectilinear coagulation (*7*) model

$$\ln\left(\frac{N_{YG}}{N_{YG}(0)}\right) = -\frac{1.3\,G}{8}(d_r + d_{YG})^3 N_r \alpha_{rec} t \tag{4}$$

where d_r is the diameter of the RB and d_{YG} is the diameter of the YG beads. Based on the diameters of the RB and YG beads, the curvilinear model correction (*8*) was 1.07 times the value of the curvilinear collision efficiency, or $\alpha_{cur} = 0.719$. Bacteria could not be separated from aggregates without altering their stickiness; therefore, values of $\alpha_{rec} = \alpha_{cur} = 0.5$ were assumed for bacteria based on maximum values of the collision efficiency of $\alpha_{rec} \approx 0.5$ found for completely destabilized spheres (*21*). From the rectilinear model, the collision frequency function between a large aggregate and a small particle in an isotropic turbulent flow can be written as

$$\beta_{rec} = \frac{1.3\,G}{8} L_a^{\,3} \tag{5}$$

The curvilinear model takes into account the forces between the impermeable colliding particles, resulting in fewer collisions than predicted by the rectilinear model. The curvilinear function is related to the rectilinear function by a factor e_{cur}

$$\beta_{cur} = e_{cur}\beta_{rec} \tag{6}$$

with

$$e_{cur} = \frac{8}{(1+\lambda)^3}\exp[4.5 + 3.5\log(\gamma) - \lambda(20.7 + 11.5\log(\gamma))] \quad (\text{for } \gamma < 1) \tag{7}$$

where $\lambda = d_p/L_a$, $\gamma = A/(18\pi\mu G L_a^3)$, A is the Hamaker constant (assumed to be 4×10^{-20} J; ref *8*), and $\mu = 0.0095$ g cm^{-1} s^{-1} is the fluid viscosity.

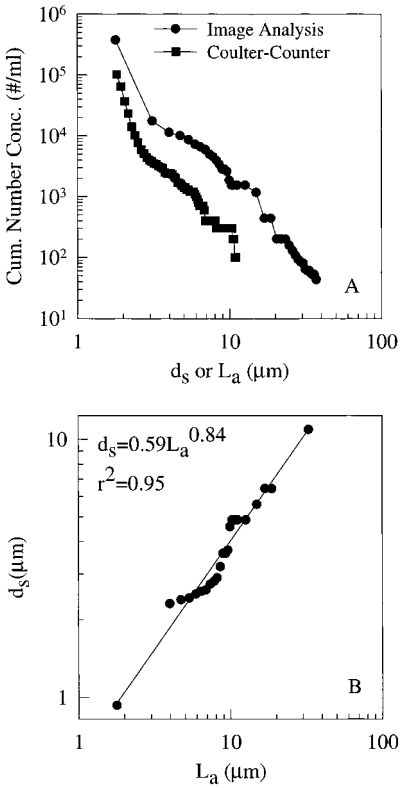

FIGURE 1. (A) Cumulative particle size distributions of bacteria measured as a solid equivalent diameter (d_s) with a Coulter-Counter and characteristic length (L_a) measured with an image analysis system. (B) Relationship between d_s and L_a for bacterial aggregates determined using the particle concentration technique.

Li and Logan (*14*) proposed a collision frequency function for collisions between large fractal aggregates ($L_a > 200\ \mu m$) with small particles as

$$\beta = 0.01 \times 10^{-0.9D} L_a^{3.3-0.63D} G^{1-0.33D} \quad (8)$$

Although fluid shear is the dominant mechanism producing collisions between particles, when the colliding particles are small, the collision frequency function caused by Brownian motion (β_{Br}) can also be included. This collision function is calculated as

$$\beta_{Br} = \frac{2}{3}\frac{kT}{\mu}\frac{(L_a + d_p)^2}{L_a d_p} \quad (9)$$

where k is Boltzmann's constant and T is the temperature. As each mechanism operates independently, the total collision frequency function can be expressed as the sum of individual collision frequencies.

Results

Fractal Dimensions of Aggregates. The cumulative number size distributions expressed in terms of length and solid equivalent diameter (Figure 1A) were used to develop a plot of L_a vs d_s (Figure 1B). Based on a slope of 0.84 ± 0.04 (±SD) in Figure 1B, the fractal dimension was calculated using eq 1 as $D = 2.52 \pm 0.12$ for the bacterial aggregates. By the same procedure, a plot of L_a vs d_s was constructed for the RB aggregates, resulting in a slope of 0.77 ± 0.06 and a fractal dimension of $D = 2.31 \pm 0.18$ (Figure 2). This value of D is in agreement with the value found by Li and Logan (*14*) (D = 2.33 ± 0.07) for larger RB aggregates using similar experimental conditions.

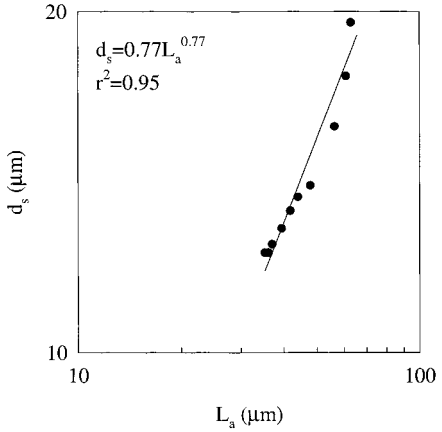

FIGURE 2. Relationship between d_s and L_a for microsphere aggregates determined using the particle concentration technique.

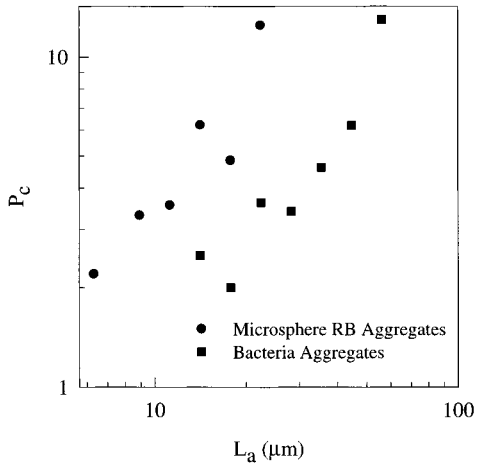

FIGURE 3. Number of YG beads captured by aggregates of size L_a in 2 min for bacteria (N_p= 1.0 × 10^7 mL^{-1}) and microsphere (N_p= 5.0 × 10^6 mL^{-1}) aggregates.

Particle Capture Rates. An example of the number of particles captured, P_c, by bacterial and RB aggregates after 2 min of coagulation is shown in Figure 3 ($N_p = 5.0 \times 10^6$ mL^{-1} for RB aggregates, and $N_p = 1.0 \times 10^7$ mL^{-1} for bacterial aggregates). While the number of particles captured increases with size in roughly the same manner for the two different types of aggregates, the total number of particles captured by the RB aggregates was greater than that captured by the bacterial aggregates, even though the number of YG beads in solution was two times smaller in the RB experiments than in the bacterial aggregate experiments.

The coagulation data obtained from seven experiments conducted at different sampling times and particle concentrations were combined by plotting the measured collision frequencies of the two different types of aggregates, P_c/tN_p, as a function of aggregate length (Figure 4). The measured P_c/tN_p increased for both types of aggregates, with a measured slope $m = 1.02$ for the bacterial aggregates (Figure 4A) and $m = 1.24$ for the RB aggregates (Figure 4B).

Collision Frequencies of RB Aggregates. The collision frequency, β, was calculated for the RB aggregates using the calculated collision efficiency, α_{cur} and compared to the results of Li and Logan (*14*) for larger aggregates coagulated at a similar shear rate (15 s^{-1}) (Figure 5). Data for RB aggregates obtained here compare reasonably well with results in Li and Logan (*14*) for microsphere aggregates over a larger size range of 200−1000 μm although the slope m is different in the two studies. Using eq 8 from Li and Logan (*14*) with $m = 3.3-0.63D$ produces $m = 1.84$ for microsphere

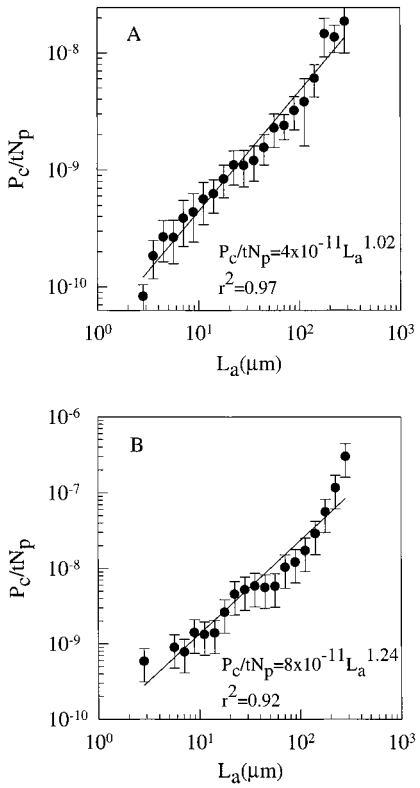

FIGURE 4. Relationship between P_c/tN_p (±SD) with L_a for experiments at different values of N_p for (A) bacterial aggregates (1.7×10^7, 3.4×10^7, and 1.0×10^7 mL^{-1}) and (B) RB aggregates (5.0×10^6, 1.4×10^6, and 3.0×10^6 mL^{-1}).

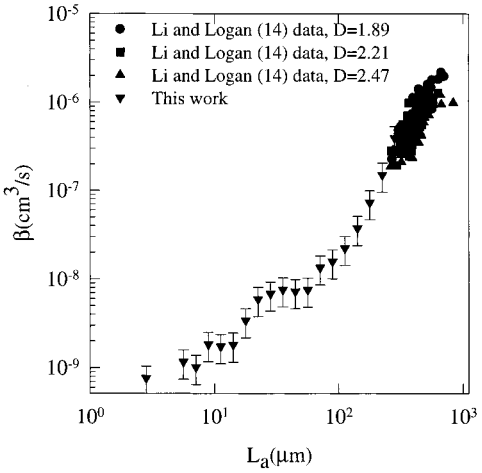

FIGURE 5. Collision frequency values found in this work (±SD) versus data for aggregates with fractal dimensions of 1.89, 2.21, and 2.47 from the experiments done by Li and Logan (*14*).

aggregates when $D = 2.31$. This slope is slightly larger than that obtained here ($m = 1.24$) for RB aggregates when the fractal dimension is included in this comparison.

Comparison of Collision Frequencies with Rectilinear and Curvilinear Models. The collision frequencies calculated using the rectilinear and curvilinear coagulation models (eqs 5−7) differ by ~7 orders of magnitude for aggregate sizes of ~100 μm (Figure 6). For smaller aggregates (3−5 μm), β approached values close to those predicted by the rectilinear and curvilinear models. When viewed over scales spanning several orders of magnitude, there is little difference between the collision functions for the RB and bacterial aggregates. However, these data are appreciably different from that predicted using the rectilinear and curvilinear models.

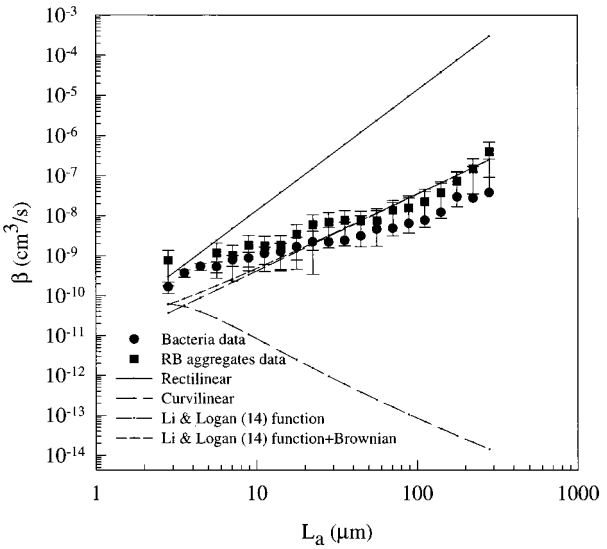

FIGURE 6. Collision frequencies calculated here for bacteria and microsphere aggregates (±SD) compared to the rectilinear (eq 5) and the curvilinear (eqs 6 and 7) collision models; fractal collision frequency function reported by Li and Logan (*14*) before and after addition of collision frequencies produced by Brownian motion (eqs 8 and 9).

Collision frequencies of both types of aggregates (both bacterial and red microspheres) with YG beads are consistent with values reported by Li and Logan (*14*) for collision frequencies for larger (L_a > 200 μm) inorganic aggregates. The curvilinear function predicts that the collision frequencies will decrease as the aggregate and small particle sized become more dissimilar. However, the opposite occurs: collisions occur more frequently as particle size increases. The increase in the collision frequency function is consistent with the prediction by the rectilinear model that collisions will increase, although the magnitude of this increase is not as large as predicted by the model. Overall, the collision frequency function of fractal aggregates 3−1000 μm in size increased from 10^{-10} to 10^{-6} cm^3 s^{-1} for aggregate collisions with small particles, in comparison to the predicted increase to approximately 10^{-3} cm^3 s^{-1} using the rectilinear model.

The largest differences between the collision frequencies measured here and those predicted by Li and Logan (*14*) occurred for collisions between small aggregates (~5 μm) and the YG microspheres. One reason for this difference could be that collisions were generated by a mechanism other than fluid shear. Because these small aggregates (~5 μm) were in the range of particle sizes for which Brownian motion could be important, the collision frequency function β_{Br} (eq 9) was included in the overall fractal collision frequency function, β, and the calculations repeated. However, it was found that the inclusion of Brownian motion had a small overall effect on the magnitude of the collision function (Figure 6). A more likely reason for the deviation of the data from the predicted fractal function is that the fractal nature of the smaller and larger aggregates was different. As aggregates sizes approached those of particles making up the aggregate, they may have started to lose their fractal scaling properties and, therefore, collided at rates different than those observed for the larger fractal aggregates.

Discussion

The substantial decrease in the collision function (4 orders of magnitude) predicted using the curvilinear collision model for aggregates of 3−300 μm was not observed here for either bacteria or microspheres. Instead, β increased (from 10^{-10} to 10^{-6} cm^3 s^{-1}) with aggregate size (3−1000 μm) as predicted

by the rectilinear model based only on projected area. The measured increase in β over this size range was not, however, as large as that calculated using the rectilinear collision kernel (10^{-10}–10^{-3} $cm^3 s^{-1}$). The fractal nature of coagulated particles results in aggregates with much higher actual surface area per projected area than for a perfect sphere of corresponding size. This larger surface area, combined with a highly porous structure that can allow streamlines to penetrate the aggregate and allow intra-aggregate advective flow (*3*, *22*, *23*), produces much higher collision rates than those calculated for impermeable spheres.

The collision frequencies measured here between microsphere aggregates and small particles overlap with those reported previously (*14*) for larger microsphere aggregates (200−1000 μm), resulting in collision rates that span a wide range of particle sizes when colliding particle sizes are dissimilar (Figure 6). Very small aggregates, ranging from the monomer size to aggregates 3 μm in size were not included in our analysis because it was not clear that these small aggregates possessed fractal scaling properties. The smallest particle size possible is the spherical monomer (not a fractal particle). The smallest aggregate that has fractal properties, known as a fractal generator, must be composed of many spheres. Therefore, there is a range of particle sizes below which the aggregate would not have the scaling properties associated with larger fractal aggregates. Although we chose a minimum of 3 μm for our smallest fractal aggregate, different scaling properties of the smaller and larger aggregates likely account for deviations of our data from the collision function of Li and Logan (*14*) measured for much larger aggregates.

The particle capture efficiency of bacterial aggregates with microspheres was smaller than that of microsphere aggregates with other microspheres. This most likely arises from three factors: (i) a lower sticking coefficient between bacteria and microspheres; (ii) a lower intra-aggregate permeability of the bacterial aggregates than for the microsphere aggregates; and (iii) the packing arrangement of particles. First, although we attempted to destabilize all particles using a coagulant, we were not able to measure a bacterium−microsphere sticking coefficient. Any attempts to break up aggregates into single cells would have damaged the cells and released intracellular material making the measurement meaningless. Breaking up the aggregate would also have released exopolymeric material from the aggregate. This exopolymeric material could itself coagulate with bacteria (*24*, *25*), altering the bacterial sticking coefficients with other particles. If α for bacterial aggregates is assumed to be ~0.2 (instead of $\alpha = 0.5$ assumed here for completely destabilized particles), the collision frequency function for bacterial aggregates would be the same as that of the microsphere aggregates. Second, the lower collision frequency function for bacterial aggregates may be due to the presence of bacterial exopolymeric material in bacterial aggregates as this material can block pores and reduce intra-aggregate flow. Finally, packing of particles in the aggregate can be important. The primary particles composing the bacterial and microsphere aggregates are different with more rod-shaped bacteria vs perfectly spherical beads for RB aggregates. This difference in particle geometry can result in different aggregate structures and lead to more compact structures for bacterial than microsphere aggregates. It is well-established for colloids formed by Brownian motion that aggregates become more tenuous with lower fractal dimensions (*26*, *20*). Thus, the more compact packing structure of bacterial aggregates is demonstrated here by a higher fractal dimension of bacterial ($D = 2.52$) than microsphere ($D = 2.31$) aggregates formed under similar hydrodynamic conditions.

These results demonstrate that fractal aggregates of particles collide much more frequently than expected based on spherical−particle coagulation models, suggesting that coagulation rates in natural systems are much more rapid than previously calculated using spherical coagulation models. Collision measurements in this and previous work (*4*, *14*), however, have only considered collisions between single, spherical particles and fractal aggregates. Clearly, many collisions will also occur between dissimilar-sized fractal aggregates, but collision frequencies between two fractal aggregates have yet to be examined. Additional research is needed to examine this more complex situation, but the high collision functions measured here make it likely that collision frequencies between fractal aggregates will be much closer to estimates produced using rectilinear than curvilinear models.

Acknowledgments

Support for this project was provided by the Comissió Direcció de Recerca (DGR) of the Catalan Government, Grant 1997BEAI200229-Annex II.

Literature Cited

(1) Alldredge, A.; Gotschalk, C. *Limnol. Oceanogr.* **1988**, *33*, 339.
(2) Fowler, S. W.; Knauer, G. A. *Prog. Oceanogr.* **1986**, *16*, 147.
(3) Logan, B. E.; Hunt, J. R. *Limnol. Oceanogr.* **1987**, *32*, 1034.
(4) Li, X.; Logan B. E. *Environ. Sci. Technol.* **1997**, *31*, 1229.
(5) Honeyman, B. D.; Santschi, P. H. *J. Mar. Res.* **1989**, *47*, 951.
(6) Smoluchowski, M. *Z. Physik. Chem.* **1917**, *92*, 129.
(7) Friedlander, S. K. *Smoke, Dust and Haze*; Wiley-Interscience: New York, 1977.
(8) Han, M.; Lawler, D. F. *J. Am. Water Works Assoc.* **1992**, *84*, 79.
(9) Chellam, S.; Weisner, M. R. *Water Res.* **1993**, *27*, 1493.
(10) Logan, B. E.; Wilkinson, D. B. *Limnol. Oceanogr.* **1990**, *35*, 130.
(11) Jiang, Q.; Logan, B. E. *Environ. Sci. Technol.* **1991**, *25*, 2031.
(12) Oles, V. *J. Colloid Interface Sci.* **1992**, *154*, 351.
(13) Lin, M. Y.; Lindsay, H. M.; Weitz, D. A.; Ball, R. C.; Klein, R.; Meakin, P. *Nature* **1989**, *339*, 360.
(14) Li, X.; Logan, B. E. *Environ. Sci. Technol.* **1997**, *31*, 1237.
(15) Li, D. H.; Ganczarczyk, J. J. *Environ. Sci. Technol.* **1989**, *23*, 1385.
(16) Li, D. H.; Ganczarczyk, J. J. *Biotechnol. Bioeng.* **1990**, *35*, 57.
(17) Logan, B. E.; Grossart, H. P.; Simon, M. *J. Plankton Res.* **1994**, *16*, 1811.
(18) Li, X.; Logan, B. E. *Deep-Sea Res. II* **1995**, *42*, 125.
(19) Li, X.; Passow, U.; Logan, B. E. *Deep-Sea Res. I* **1998**, *45*, 115
(20) Logan, B. E. *Environmental Transport Processes*; Wiley: New York, 1999.
(21) Birkner, F. B.; Morgan, J. J. *J. Am. Water Works Assoc.* **1968**, *60*, 174.
(22) Adler, P. M. *J. Colloid Interface Sci.* **1981**, *81*, 531.
(23) Logan, B. E.; Hunt, J. R. *Biotechnol. Bioeng.* **1988**, *31*, 91.
(24) Alldredge, A. L.; Passow, U.; Logan, B. E. *Deep-Sea Res.* **1993**, *40*, 1131.
(25) Passow, U.; Alldredge, A. L.; Logan, B. E. *Deep-Sea Res.* **1994**, *41*, 335.
(26) Schaefer, D. W. *Science* **1989**, *243*, 1023.

Received for review November 2, 1998. Revised manuscript received March 29, 1999. Accepted April 16, 1999.

ES981125V